A&A 412, 541–553 (2003)
DOI: 10.1051/0004-6361:20031435

Astronomy & Astrophysics

Fast photospheric flows and magnetic fields in a flaring active region

N. Meunier[1] and A. Kosovichev[2]

[1] Observatoire Midi-Pyrénées, 57 avenue d'Azereix, BP 826, 65008 Tarbes Cedex, France
[2] Hansen Experimental Physics Laboratory, Stanford University, Stanford, CA 94305, USA
e-mail: sasha@khors.stanford.edu

Received 25 June 2003 / Accepted 3 September 2003

Abstract. We present new results from the coordinated observations between the THEMIS telescope (in the multi-line spectropolarimetric mode) and Michelson Doppler Imager (MDI) on SOHO obtained in November 2000 for active region NOAA 9236 which was the source of several X-class flares. The goal of these observations was twofold: to verify MDI measurements of the line-of-sight components of flow velocity and magnetic field, and to obtain more information about the photospheric flows and magnetic fields in flaring regions. Using the simultaneous observational data in several lines we have analyzed the structure and dynamics of this active region at the photospheric level before and after a X4.0 flare of November 26, the last major flare produced by this very active region. Vector magnetic field maps are computed from the THEMIS data by full inversion of the Stokes line profiles. In the Doppler velocity maps from THEMIS and MDI, we observe fast photospheric flows which appear to be supersonic in two regions located close to the region where the flare occurred. These flows seem to be long-lived (several hours at least). In one position, we observe a supersonic downflow strongly inclined with respect to the vertical (by 51°), while in another position, a flow suggesting a strong shear with a supersonic component as well, although almost horizontal upflows and downflows cannot be ruled out in that case. These flows seem to be present at least 8 hours before the flare, and the amplitude in the second case appeared to be modified during the flare, especially, during the first minutes. In the MDI data, we observed strong permanent changes of the longitudinal magnetic flux, associated with the flare. The role of the strong flows and their interaction with the magnetic field in the development of the active region and the flare is not understood yet.

Key words. Sun: magnetic fields – Sun: flares – Sun: photosphere – Sun: activity

1. Introduction

Observations of photospheric magnetic fields and flows as well as plasma thermodynamic properties in flaring active regions are important for understanding the mechanisms of energy storage and release. Despite the long history, these observations have not produced a clear picture of the flare processes in the photosphere. Severny (1958) first discovered that solar flares tend to occur in the vicinity of neutral lines separating regions with opposite polarities of the line-of-sight (LOS) magnetic field components, and where the field gradient is particularly strong (of the order of 1 G/km). Martres & Soru-Escaut (1977) argued that flares were often associated with the neutral line of the line-of-sight velocity. Several observers found significant upflows in the photosphere prior some flares (e.g. Yoshimura et al. 1971; Harvey & Harvey 1976). More recent observations (Keil et al. 1994) revealed strong horizontal and shearing flows near flare kernels. However, the role of the photospheric flows and magnetic fields in the mechanism of solar flares is still not understood.

The space observations from Michelson Doppler Imager (MDI) on SOHO (Scherrer et al. 1995) provide an unique opportunity to study the structure and variations of the LOS magnetic field and flows in flare regions. However, the LOS information from a single line is insufficient for physical interpretation of these observations (Kosovichev & Zharkova 2001). Also, the MDI measurements, obtained from a sequence of filtergrams taken in four positions across the spectral line, suffer from saturation in the case of strong flow velocity and field strength, and also may be not sufficiently accurate when rapid changes, on the a few minute scale, occur. Therefore, it is highly desirable to combine the MDI data with spectral ground-based observations of solar flare. In this paper, we report about one of the first attempts of such coordinated observations which were carried as a part of the SOHO Joint Observing Programs.

We have performed spectropolarimetric observations of a flaring active region at the photospheric level using the THEMIS telescope. Our objective is to describe the complex

Send offprint requests to: N. Meunier,
e-mail: meunier@bagn.obs-mip.fr

topology of this active region by using vector magnetic field measurements, investigate mass flows, and study the variations of magnetic field and flows, associated with a strong flare. We also study the spectral characteristics in the flare region, and, particularly, unusual V and Q Stokes spectra. The outline of this paper is the following. In Sect. 2 we describe the coordinated THEMIS and MDI observations on SOHO, as well as also additional Hα observations obtained at the CU Cesco Station in Argentina. The processing of THEMIS data is described in Sect. 3. In this paper we use the multi-line capabilities of THEMIS mostly to confirm that the strong flows we observe are not an observational bias. The precise comparison between the different wavelengths will be the subject of a future paper. Analysis of the results is made in Sect. 4: We describe the general evolution of the region and then emphasize the strong flows which are observed in both THEMIS and MDI data. These new results are summarized and discussed in Sect. 5.

2. Observations

2.1. THEMIS: Multi-line spectropolarimetry

Observations were performed using the multi-line spectropolarimetric mode (MTR) of THEMIS telescope. This mode, described by Paletou & Molodij (2000), allows simultaneous I+Stokes and $I-$Stokes observations. The field of view was ∼110 arcsec in the direction along the 0.5 arcsec wide slit. We observed sequences of Stokes parameters $[Q, -Q, U, V]$ to allow for a beam exchange analysis. It took ∼6 s to record such a sequence on 6 cameras (3 spectral domains). In this paper, we focus on three observations of active region NOAA 9236, that are summarized in Table 1.

The two scans of this region were performed with a step of 0.8 arcsec and the time exposure of 800 ms. The first scan was made during a better seeing period (in the range of 1–2 arcsec). The angle between the normal to the solar surface and the line-of-sight was ∼41° at the center of the region (on Nov. 26). In addition, spectropolarimetric observations at a fixed position were carried out near the end of the Hα emission of the X4.0 flare occurring between 16:38 and 17:32 on Nov. 26 (see Fig. 1). The exposure time was 600 ms. During these observations, the Sun was rather low, about 9° above the horizon, and the seeing was poorer (several arcseconds).

In all cases, the flat-field measurements were made using an elliptical motion of the telescope in a quiet region around disk center. The slit was oriented toward the celestial North. The spectral resolution was between 18.5 and 22.8 mÅ per pixel depending on the wavelength.

The line characteristics are described in Table 2. The Fe I 6301.5 and 6302.5 Å lines have characteristics only slightly different from the Ni line, but the 5635.8 and 5634.0 Å lines are formed much deeper in the photosphere. One should note that other values for the line formation height have been published, for example the value of ∼200 km for the Ni I 6767.8 Å line by Jones (1989). The difference between this last computation and the results of Table 2 could be due to slightly different computation method, in particular the physical quantity for which the response functions are computed. Therefore it is important to compare line formation heights with computations made in similar conditions, as in Table 2. One should also keep in mind that these line formation heights are averaged over a larger distribution and therefore provide only an approximation.

Table 1. Characteristics of THEMIS observations: Set 1 is [Fe I 6302.1 Å and 6302.5 Å, Fe I 5576.1 Å, Ni I 6767.8 Å], set 2 is [Fe I 6302.1 Å and 6302.5 Å, Ni I 6767.8 Å, Fe I 5635.8 and 5634.0 Å]. The indicated time corresponds to the starting time of the observation. A *scan* means that the whole region has been observed. The *fixed* position corresponds to the slit positioned as indicated in Fig. 2.

Date	Time	Length	Type	Wavelength
25 Nov. 2000	8:34	29 min	scan	set 1
26 Nov. 2000	8:24	29 min	scan	set 1
26 Nov. 2000	17:20	12 min	fixed	set 2

Table 2. Spectral line characteristics for the wavelength used in this paper. Lande factors are courtesy of J.-F. Donati. The line formation heights above the photospheric level are computed from the LTE response functions at the disk center for the atmosphere model VAL-C (K. Puschmann, private communication).

Wavelength (Å)	Landé factor	Formation height
6302.5	2.487	281 km
6301.5	1.669	400 km
6767.8	1.426	374 km
5635.8	0.677	153 km
5634.0	1.425	22 km

2.2. MDI/SOHO: Full-disk magnetograms and Dopplergrams

The THEMIS observations were coordinated with MDI/SOHO observations, which provide maps of the line-of-sight component of the magnetic and velocity fields (Scherrer et al. 1995). The MDI observations are made in the Ni I 6767.8 Å spectral line, which was also used for THEMIS observations (see Table 2). We used MDI in the full-disk mode (FD) from Nov. 26 (8:00) to Nov. 26 (24:00), with a temporal cadence of 1 min (the pixel size is 2 arcsec). The observed active region has been tracked to remove the displacement caused by solar rotation.

2.3. OAFA: Full disk Hα images

We have analyzed Hα full-disk images obtained with the Hα telescope from the CU Cesco Station at the Observatorio Astronómico Félix Aguilar (OAFA) in Argentina between 16:00 and 18:00 UT on Nov. 26, 2000. The data are available with a temporal cadence of approximately 12 s and a relatively low spatial resolution, significantly lower than 2.1 arcsec defined by the pixel size. The intensity level reached a saturation level in the flare region. Unfortunately

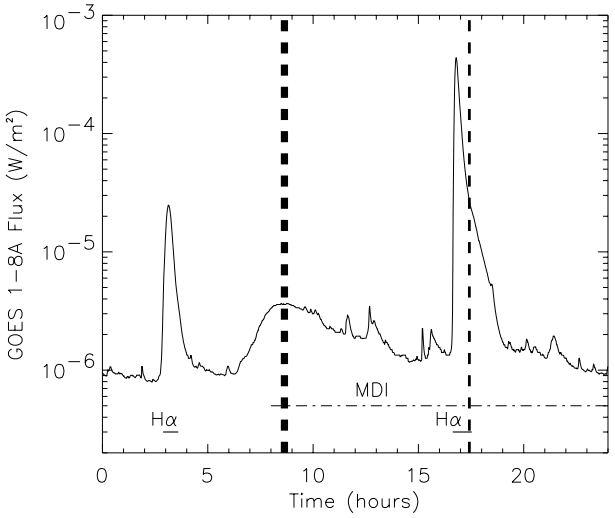

Fig. 1. GOES X-ray flux in the range 1–8 Å for Nov. 26, 2000. The first flare (from 2:47 to 3:20 UT) is an M2.2 flare with a total energy of 4×10^{21} J and is located around latitude 19° and longitude 30° while the second one (from 16:34 to 16:56) is a X4.0 class flare with a total energy 10 times larger and is located around latitude 18° and longitude 38°. The thick vertical dashed line indicates the time of the THEMIS scan (Nov. 26, 8:24) and the thin dashed line shows the time of the fixed position THEMIS observation (Nov. 26, 17:20). The thickness of these lines is proportional to the duration of the observation. The duration of Hα flares are indicated by 2 small horizontal lines. The long horizontal dotted-dashed line corresponds to the MDI observations used in this paper.

10 min of the Hα data simultaneous with our THEMIS observations were lost because of clouds (Nov. 26, 17:20).

3. THEMIS data processing

3.1. Stokes parameter computation

The main steps of the THEMIS data analysis are the following:

(i) *Flat-field and line curvature correction*. For each Stokes parameter of the averaged flat-field, we compute the spectral line curvature. After a correction of the curvature, a mean spectral profile is computed. The flat-field images are normalized by this profile to remove the spectral signatures and shifted back to the initial line curvature. The scan spectra are corrected for the flat-field before the curvature correction, which is then performed using the curvature values computed for the flat-field.

(ii) *Shift in x (wavelength) and y (spatial)*. The shift in wavelength (x coordinate) is computed using a profile averaged over each spectrum. A cut in the slit direction averaged over the continuum is used to compute the spatial shift (y coordinate). For these calculations we use a cross-correlation of the granulation signal.

(iii) *Beam exchange computation*. We compute the Stokes parameters using the beam exchange technique: Stokes Q is computed separately for each optical path using two spectra taken at a different time, and, then, the two resulting Q spectra are averaged. For Stokes U and V, the technique is similar except that the Q measurements are also used, i.e. we need 3 spectra for each optical path (during our observations the beam exchange was possible for one Stokes parameter only, see Sect. 2.1).

Table 3. Polarization phase versus wavelength for the analyzer plates (Characteristics and code kindly provided by F. Paletou).

Wavelength (Å)	Phase (degrees)
5576	93.18
5636	92.95
6302	89.71
6768	86.99

(iv) *Crosstalk corrections*. Although THEMIS is a polarization free instrument, the quarter wave plates are not perfect for all wavelengths, and the polarization phase can be off by several degrees (see Table 3). The amplitude of the crosstalks reaches a few percents for some of our wavelengths.

(v) *Zero corrections*. Due to the problem of "co-spatiality" between the two slits described in more detail in the next section, the simultaneous spectra of I+Stokes and I−Stokes (see Sect. 2.1) do not correspond to the same position on the Sun. As a consequence there are residuals in the continuum of the Stokes spectra, especially in the U profiles. This represents a problem for inversions. Therefore, we have subtracted the observed zero from the data, modulated by the I profile.

(vi) *Line-of-sight components computation*. Maps of LOS magnetic and velocity fields are obtained using the center-of-gravity method (Rees & Rayrole 1979) applied to the $I \pm V$ spectra. Results are shown in Fig. 2 for the two scans of the region.

(vii) *Vector magnetic field computation*. This is performed over the whole field of view using a computer code kindly provided by T. Metcalf. This code, described by Jefferies et al. (1989), is routinely used at the Mees Observatory (University of Hawaii) for preliminary data reduction of the Haleakala Stokes Polarimeter data. It is based on the weak-field approximation and does not perform a full inversion. The 180°-ambiguity of the azimuth is solved using the same code (see, e.g. Canfield et al. 1993), as well as the projection effects. The maps are very similar for the Ni and Fe lines. A full inversion of the interesting profiles has also been performed using the inversion code described in Fruttiger (2000). This code allows to consider models with any number of structural components (magnetic or not) and takes into account variation of the model parameters with height.

3.2. Main limitations

We summarize here some limitations of our THEMIS observations in addition to the crosstalks and zero corrections mentioned above (some of them are discussed by López Ariste et al. 2000):

(i) *Cospatiality*. The polarimeter is followed by a calcite beam splitter and two slits to allow the simultaneous analysis of I+Stokes and I−Stokes (see Sect. 2.1). As a consequence, the two slits must be adjusted with great precision to allow observations of the same position on the Sun. Unfortunately, this did not work well during these observations; there was a difference of 0.23 arcsec between the two beams, because the

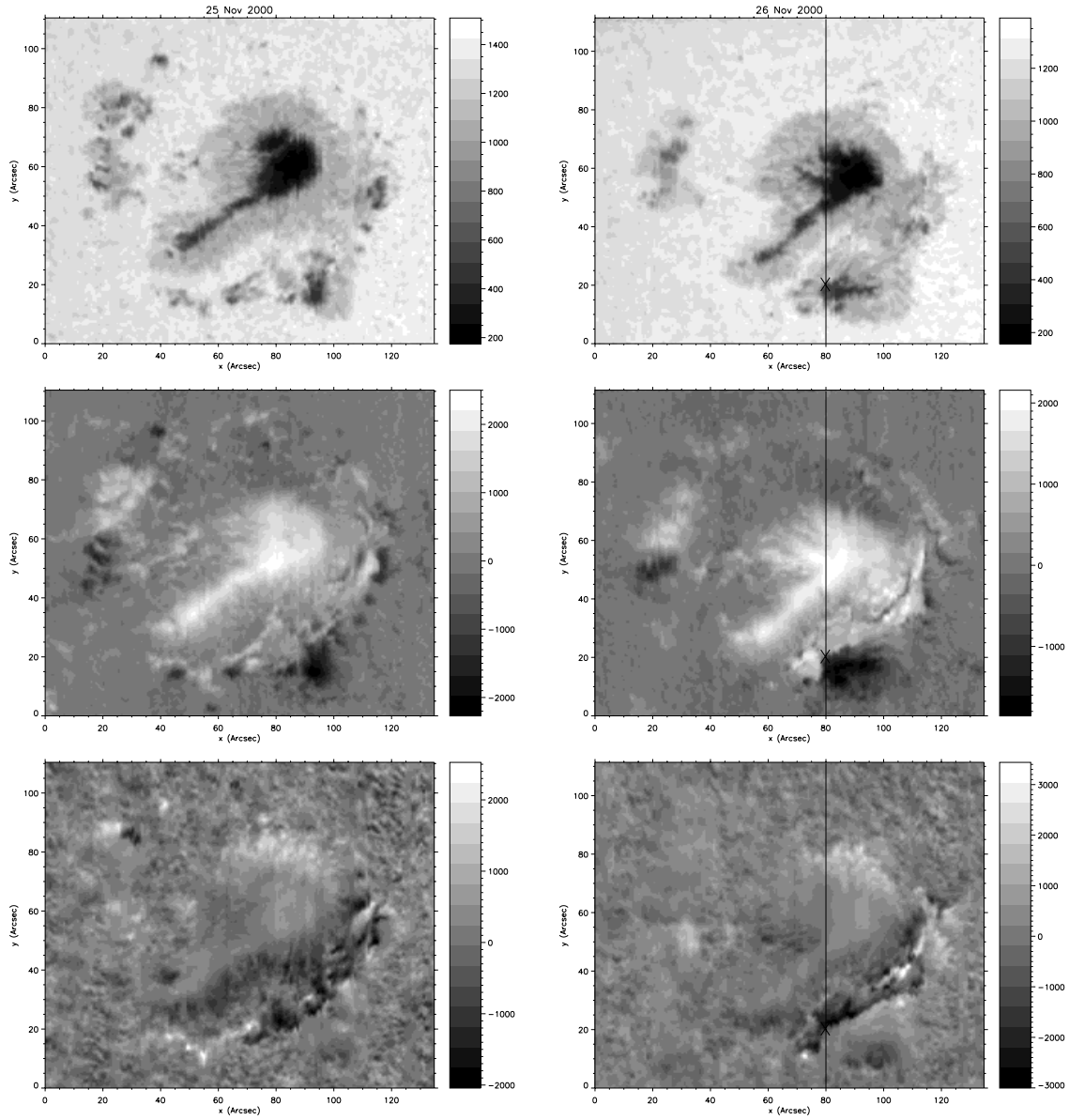

Fig. 2. Maps of continuum intensity (*top*), line-of-sight magnetic field (*middle*) and velocity (*bottom*) observed with THEMIS using the Ni line, for Nov. 25 (8:34 UT) and Nov. 26 (8:24 UT) scans. The vertical line shows the approximate position of the slit during the fixed position at the time of the flare. The cross corresponds to the plot in Fig. 10 (left). The top corresponds to the celestial North.

instrument configuration did not allow a good precision for this adjustment. This problem and its influence on spectropolarimetric precision are discussed by Meunier et al. (2002).

(ii) *Image motion and seeing*. There is no image stabilization in the telescope. The actual spatial resolution for the fixed position spectra after averaging is of the order of 1.5 to 2 arcsec. The scan spectra have a better spatial resolution, but stronger contaminated by Doppler residuals (no averaging is done).

(v) *Absolute wavelength*. There is no absolute wavelength calibration. Therefore, the zero level of the longitudinal velocity is not known precisely (an uncertainty of 100 to 200 $\mathrm{m\,s^{-1}}$ is likely). Furthermore, the spectra between the two paths have to be shifted as well as each image of a series for a given path because a trend with time is observed. The presence of magnetic field introduces some noise in this computation, and this is taken into account in the data reduction.

(vii) *Atmospheric refraction*. The various wavelengths are observed simultaneously with THEMIS. However, because of the atmospheric refraction, the observations are not at the same position on the solar surface. If the slit is perpendicular to the horizon, a shift along the slit is sufficient to correct for this problem, with only a small loss in the field-of-view. However, if the slit is not perpendicular to the horizon (and this was the case for these observations, especially for the flare data obtained at 17:20), then the interpretation becomes more difficult. For example, for our flare observations, the 5635.8/5634.0 Å lines correspond to a position more than 1 arcsec away from the 6767.8 Å line, with the 6301.5/6302.5 Å lines in between.

Other limitations are due to magnification and focus differences (the adjustments are made with a precision of 0.5% for the magnification for example) and to uncertainties in pixel size

calibrations. They can limit the precise comparison between wavelengths.

4. Results

4.1. General description of the evolution of AR 9236

The observed region, illustrated in Fig. 2 (THEMIS) and Fig. 3 (MDI) contained a roundish spot with an extension in the approximate direction towards the disk center. It had magnetic type $\beta\gamma$. The spot was of the positive (leading) polarity. The opposite polarity region (following polarity) constituted of plages only and is not visible on these maps (it is located East to the observed region). On Nov. 22, some small spots of opposite polarity appeared West of the large spot. The location of emerging magnetic flux of the opposite polarity moved later toward South: on Nov. 25 and Nov. 26, the opposite polarity spots were located mainly South to the main spot. This region has been very active over 3 days, Nov. 24–26, producing big flares on the last day of this run. Most of these large flares produced CMEs.

In this paper, we concentrate on the evolution of the region on Nov. 26 during 16 hours starting at 8:00 UT, and on the flare which started at 16:38 UT in Hα intensity (see Fig. 1). Figure 4 shows contours of the Hα intensity shortly after the beginning of the flare superimposed on the maps of magnetic and velocity fields from MDI (the South part of the active region). The Hα emission covered a wide region with the angular size of more than 1 arcmin and was located close to the small spot of the opposite polarity and to the neutral line. It overlapped with the region where strong velocity flows of both signs are found. In particular, the brightest part of the flare was close to the strong positive velocity flows. The variations of the magnetic and velocity fields occurred mostly in these regions, as can be seen from the rms value of the magnetic field and velocity signals for the 16 hours of the MDI data for each CCD pixel (Fig. 4). Figure 2 displays maps of the LOS components for the scans made on Nov. 25 and Nov. 26, revealing completely different magnetic and velocity patterns South of the main spot, between the two observations separated by 24 hours.

More details of the evolution of the line-of-sight magnetic flux are shown in Fig. 5 separately for positive and negative polarities for selected regions. For the whole active region shown in Fig. 3 (which includes the main spot with surrounding opposite polarity small spots), the positive magnetic flux was decreasing steadily starting at least 8 hours before the flare, while the negative magnetic flux was slowly increasing.

At the time of the flare, a sharp increase of the positive magnetic flux by 10^{21} Mx is observed during at least 1 hour. The flux continued to vary after the end of the flare. The negative flux, however, decreased abruptly at the beginning of the flare by 0.5×10^{21} Mx, and then continued to decrease more slowly. In region 1, we observe a similar evolution at the time of the flare, which is consistent with the fact that most of the evolution related to the flare occurred in this region. However most of the variation observed before the flare in the whole active region occurred somewhere else because the flux was quite constant in region 1 before the flare. A third of the positive flux increase was observed in region 2, and another third in region 3, although the increase was more gradual in the latter. On the other hand, the negative flux was decreasing mostly in region 3.

We note that a strong variation of the magnetic field in one pixel could correspond to flux emergence, flux cancellation, or motions of magnetic structures (or of the neutral line). Because MDI measures only the line-of-sight component of the magnetic field, the observed variation could also be caused by changes of the inclination of the magnetic field lines. In some cases, the slow change of the line-of-sight flux could be caused by solar rotation. For instance, the relative changes of the whole-region flux, shown in top panels of Fig. 5, before the flare, $|\mathrm{d}\log|B|/\mathrm{d}t| \simeq 2 \times 10^{-6}$ s^{-1}, are comparable with the maximum change of 2.7×10^{-6} s^{-1}, due to the projection effect. However, in the case of region 2 (middle left panel in Fig. 5), the flux decrease rate before the flare was much stronger, $\simeq 1.2 \times 10^{-5}$ s^{-1}, and must be related to changes in the magnetic field structure in the flaring region.

In addition, MDI observations of the line-of-sight magnetic fields, which are obtained from nine filtergrams taken with 3-s cadence, can be affected by rapid variations of the line profile and intensity due to the photospheric heating in the region of the flare. However, these effects can be significant only for rapid transient variations in the MDI signals. Clearly, the permanent changes that have been observed during the flares and never restored after the flares for the whole period of observations lasting hours and days, cannot be explained by flare heating which does not last that long. Also, unlike traditional magnetographs, MDI accounts for the variations of the line intensity that are slower than the 30-s measurement time. Therefore, the permanent changes of the line-of-sight magnetic signal detected by MDI certainly result from the structural changes of magnetic field related to solar flares. However, the transient impulsive variations in the MDI magnetic signal may be affected by the line-profile variations. These impulsive magnetic signals correlate spatially and temporally with hard X-ray impulses and, therefore, are likely be caused by direct hits of the photosphere by high-energy particles (Kosovichev & Zharkova 2001). Whether these effects are mostly of the thermal or electromagnetic nature is not known yet. Simulations of the MDI measurements for some of the impulsive events published by Kosovichev & Zharkova (2001) showed that the thermal effects can be responsible only for a relatively small portion of the observed variations. We note that a detailed discussion of these effects is beyond the scope of our paper; a complete interpretation requires high-cadence observations of the Stokes profiles of the Ni I 6767.8 Å line for such events, which are not yet available.

In the next section, we will investigate in detail two small regions of interest defined in Fig. 4, as regions 2 and 3. These regions are characterized by strongest variations of magnetic fields and the largest velocity flows, and also showed the most unusual Stokes profiles in the THEMIS data. Region 2 exhibits a strong stationary downflow (positive) velocity flow (corresponding to redshift of the spectral line), while strong flows, directed both up and down, are observed in region 3, especially at the time of the flare.

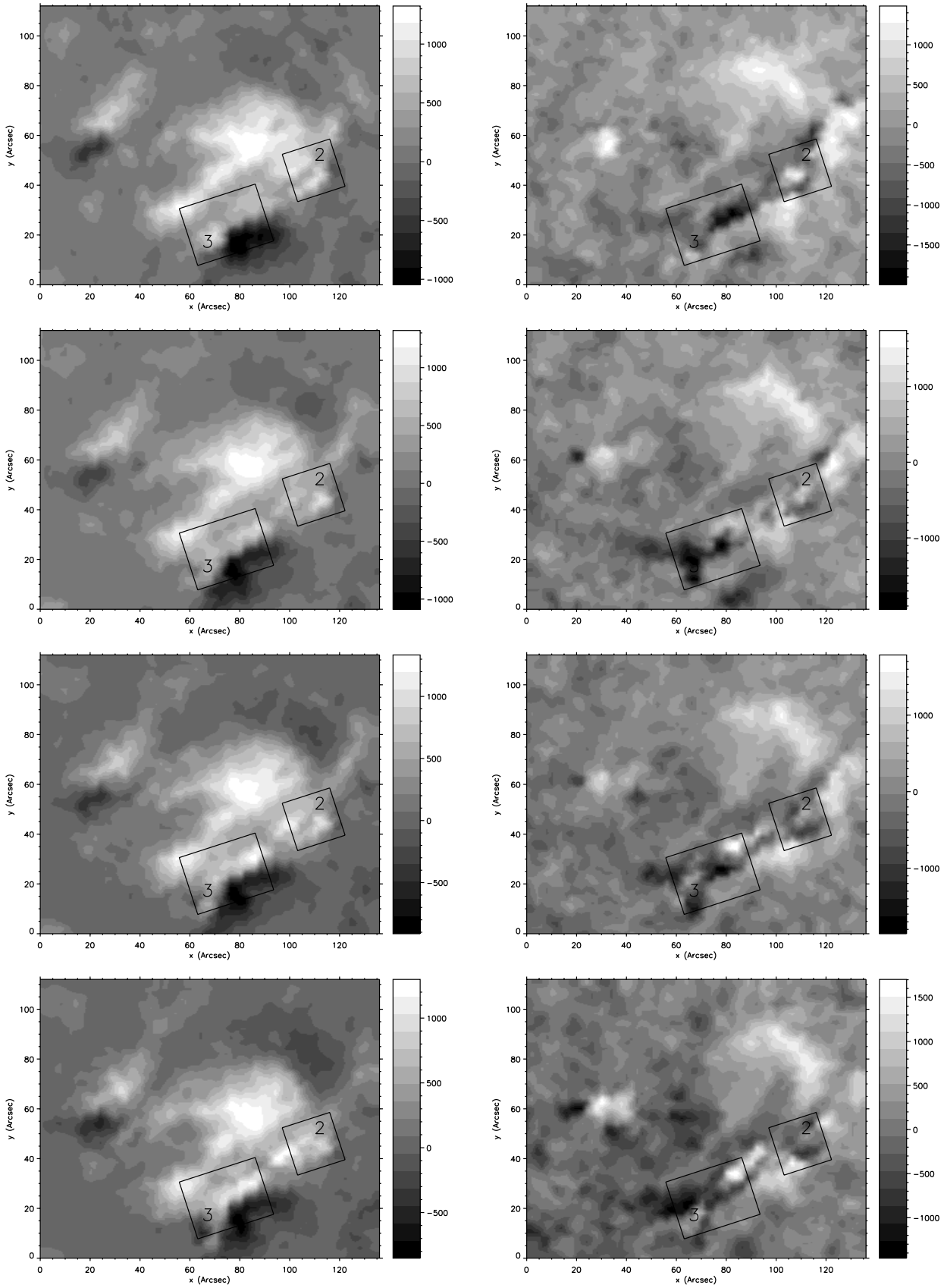

Fig. 3. MDI line-of-sight magnetic field (*left*, in G) and velocity field (*right*, in m s^{-1}) at four different times (*from top to bottom*): 10:00, 15:38 (one hour before the beginning of the Hα flare), 19:02 (~1.5 hour after the end of the Hα flare), and 24:00 UT (Nov. 26, 2000).

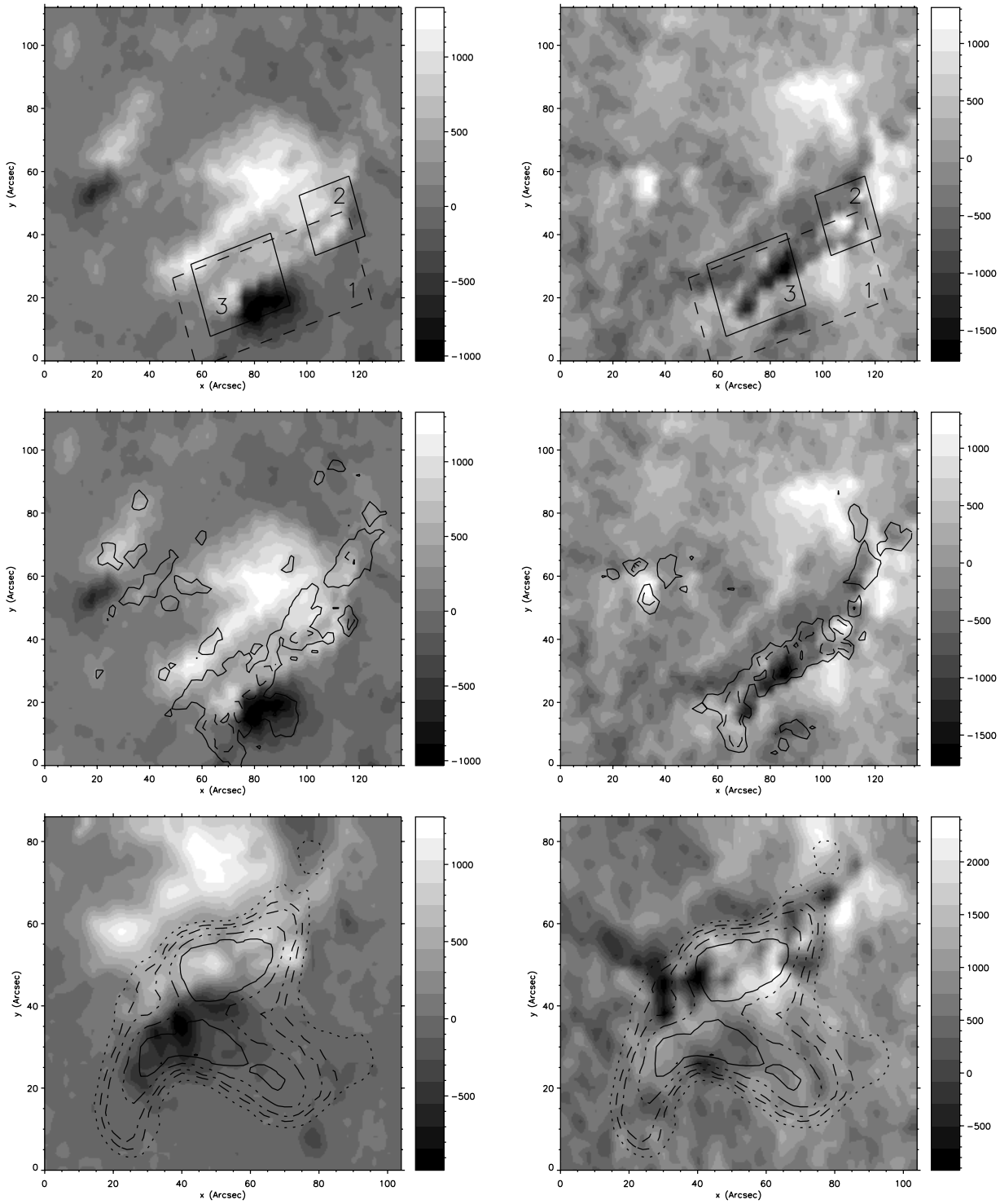

Fig. 4. *Top*: Map of the line-of-sight magnetic field component (*left*, in G) and Doppler velocity field (*right*, in m s^{-1}) observed by MDI (Nov. 26, 2000, 8:00 UT). Boxes indicate regions that are investigated in detail in the paper. Positive velocity is redshifted (shown in light color). The images have been rotated to match the orientation of THEMIS data. *Middle*: Same maps, with contours of the rms magnetic field (*left*, solid line 100 G, dashed line 200 G) and velocity field (*right*, solid line 300 m s^{-1}, dashed line 500 m s^{-1}) in each pixel. *Bottom*: Map of the line-of-sight components of magnetic field (*left*, in G) and velocity field (*right*, in m s^{-1}) observed with MDI at 16:46 UT (i.e. close to the beginning of the flare) on a smaller field of view, on which are superimposed several Hα intensity contours from 3500 to 6700 ADU (Analog Digit Unit).

4.2. Analysis of region 2

4.2.1. Observation of a supersonic flow

A very interesting feature in the Nov. 26 scan of the region made by THEMIS (Fig. 2) is a very strong downflow (redshifted), clearly visible in the Stokes *V* spectrum shown in Fig. 6. This figure also shows the location of this region, which corresponds to the relatively large flows observed in MDI region 2 in Fig. 7 at the same time (around 1400 m s^{-1}). However, the signal observed in the THEMIS data correspond

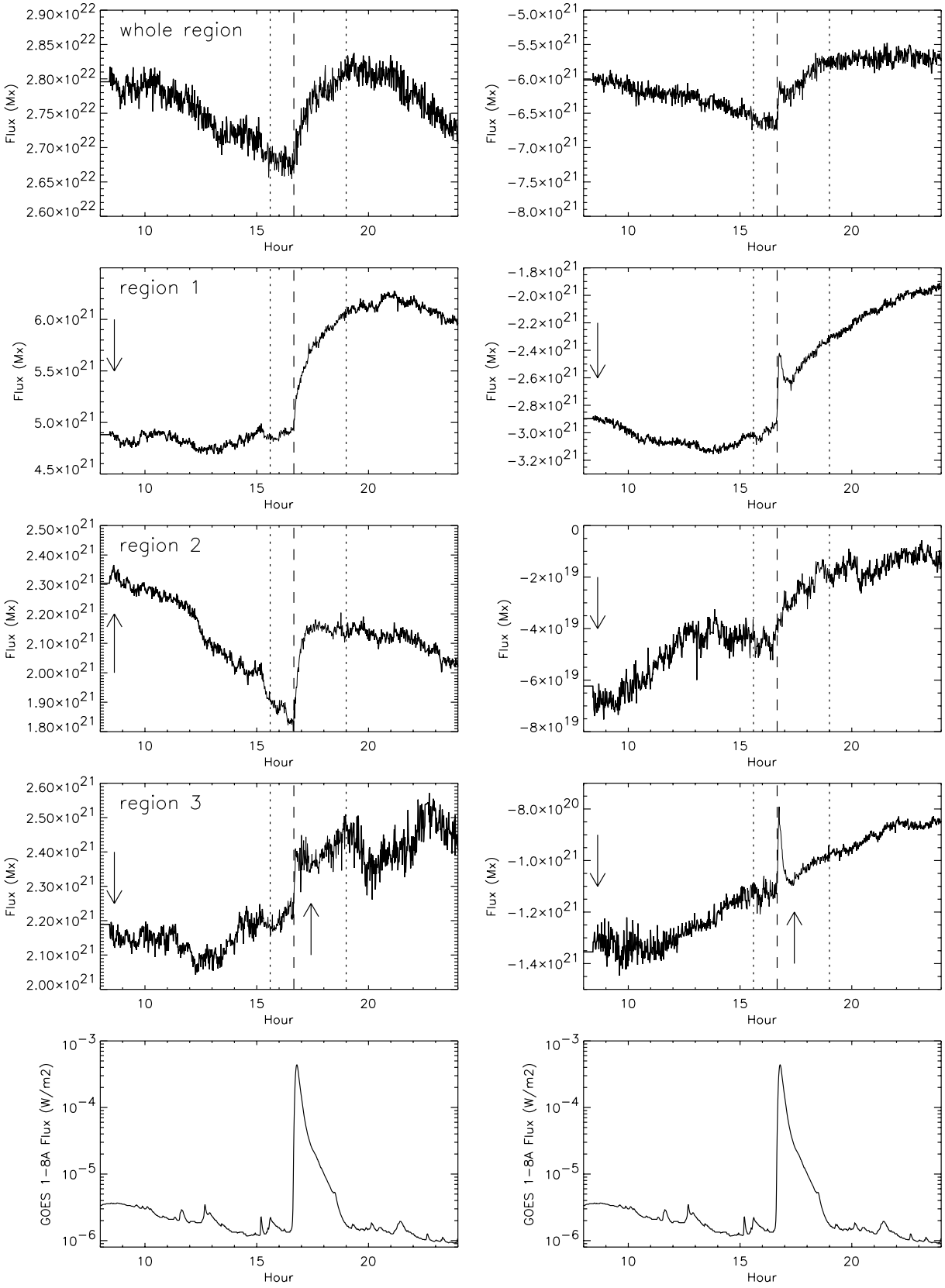

Fig. 5. *Top plots* (four rows): Positive (*left*) and negative (*right*) magnetic flux in different regions of the field of view (numbers refer to regions defined in Fig. 4). The vertical dashed line marks the beginning of the Hα flare. The dotted line correspond to one hour before the beginning of the Hα flare and to 1.5 hour after its end. The arrows indicate that the region has been observed with THEMIS at that time. The projection effects are small. *Bottom*: GOES X-ray flux in the range 1–8 Å for comparison (same as Fig. 1).

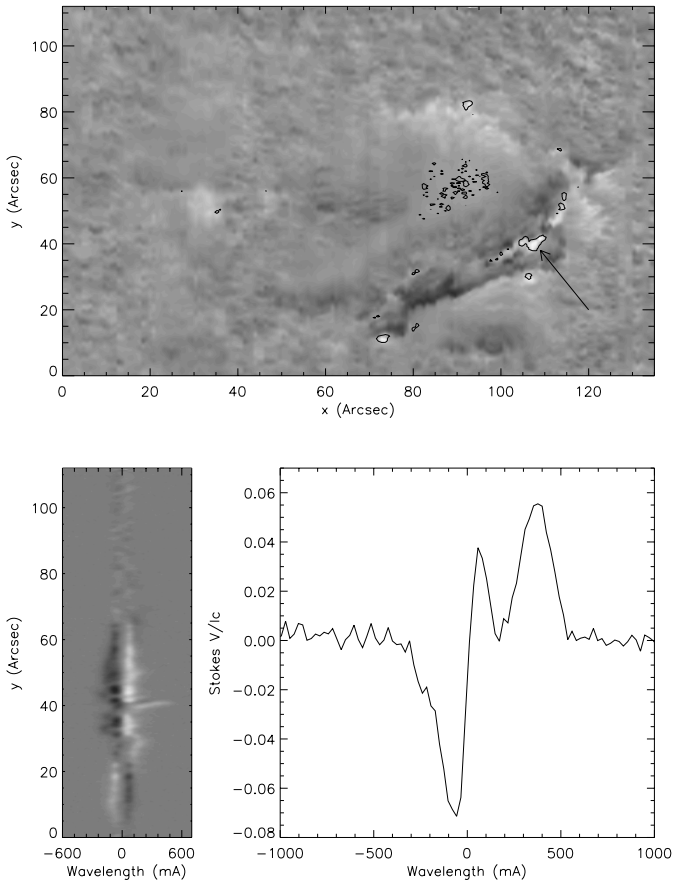

Fig. 6. Contours (*top*) show regions where the amplitude of Stokes V is large at ∼300 mÅ from the line center (at zero LOS velocity), superimposed on a map of LOS velocity field (Ni line) made at THEMIS on Nov. 26 (8:24 UT). Note that in the center of the spot, the structures correspond to some Zeeman signal due to some weak lines. We are mainly interested in the region pointed by the arrow. An example of V spectra (position $x = 105$ arcsec) across this region is shown at the *bottom left*. A cut through V around position $y = 40$ arcsec shows an abnormal profile (*bottom right*). Heliographic North is ∼18° CCW from the top.

to a signal much further from the line center than could be measured by MDI. We can fit such a profile with an unshifted "normal" V profile added to a strongly redshifted (10 km s^{-1}) "normal" V profile of the same polarity. The resulting LOS flow is therefore supersonic: the sound speed in the photospheric layers is about 6–7 km s^{-1} (Kentischer & Mattig 1995). This flow occupies a 5×2 arcsec^2 region, and is resolved in our data. It is also mostly observed in Stokes V, while almost no signal is visible in Stokes Q and U. The center-of-gravity method applied to the same THEMIS data shows a flow of only 3 km s^{-1}, close to what is provided by MDI observations (it is larger by a factor two, probably due to the better spatial resolution in THEMIS observations). This feature is visible at all wavelengths. A strongly redshifted signal is also seen in Stokes I, including for the 5576.1 Å line. Since this line is not sensitive to the magnetic field, we can rule out abnormal behavior of the magnetic field to explain these observations. Thus, this is very likely to be due to a real strong Doppler redshift.

4.2.2. Inversion and magnetic topology of region 2

From the THEMIS Stokes spectra, we compute vector magnetic fields using the weak-field method described in Sect. 3.1. The results are shown in Fig. 8. The average inclination (in the local frame of reference) in the strong flow zone is 51°, and, therefore, the field lines are significantly inclined with respect to the vertical (0°) in this zone. If the flow is following the magnetic field then these supersonic flows are also inclined with respect to the vertical. Note that even without the knowledge of the inclination, we can conclude that these flows are supersonic. The azimuth is in the range $[40°, 60°]$ (i.e. the field line are approximately in the North direction). We have also performed full inversion of Stokes profiles in that region, using two magnetic components (in addition to one non-magnetic component). We did not include any depth-dependence except for the temperature as it did not improve our fits significantly. The polarity of the shifted component has the sign of the main polarity in the region. We find differences in the inclination for the two magnetic components in the range $[-30°, 30°]$ and differences in azimuths between 0 and ∼30°. This means that the region exhibits a complex magnetic topology.

4.2.3. Temporal evolution of the flow

We were able to obtain only one spectropolarimetric observation of this strong flow with THEMIS. The scan made the day before did not show any similar behavior. Therefore, the THEMIS observations alone do not tell us anything about the temporal characteristic of this supersonic flow. However, the strong redshifted flow observed by MDI at the same location (Fig. 7) and at the same time corresponds to the same flow (although, of course, it is underestimated due to the MDI magnetograph-type technique). This flow, of the order of 1400 m s^{-1}, is remaining until the beginning of the flare as shown in Fig. 7 (top-right of the figure). The strong flow observed after the flare may correspond to a different structure since this flow slowly decayed throughout the day, as follows from Fig. 3. This observation suggests that the strong supersonic downflow observed with THEMIS is long-lived (at least 8 hours), and that we observed its decaying phase. Note that there were also strong blueshifted flows in that region 1.5 hour before the flare the maximum amplitude of the negative velocity (blue shift), which reached a peak of almost 2 km s^{-1}. This means that there was a very strong shear flow before the flare.

4.3. Analysis of region 3

4.3.1. Line-of-sight magnetic and velocity fields

Region 3 (shown in Fig. 4) also exhibits strong plasma flows observed in the MDI data. This region was observed twice with THEMIS on Nov. 26: first, on a scan of the region made on the morning of Nov. 26, and, then, at the end of Hα flare. In this latter observation, the slit was at a fixed position (shown in Fig. 2) during 12 min. THEMIS LOS magnetic and velocity fields as well as the continuum intensity during the last 12 min of the flare are shown in Fig. 9 for the Ni line. The other wavelengths

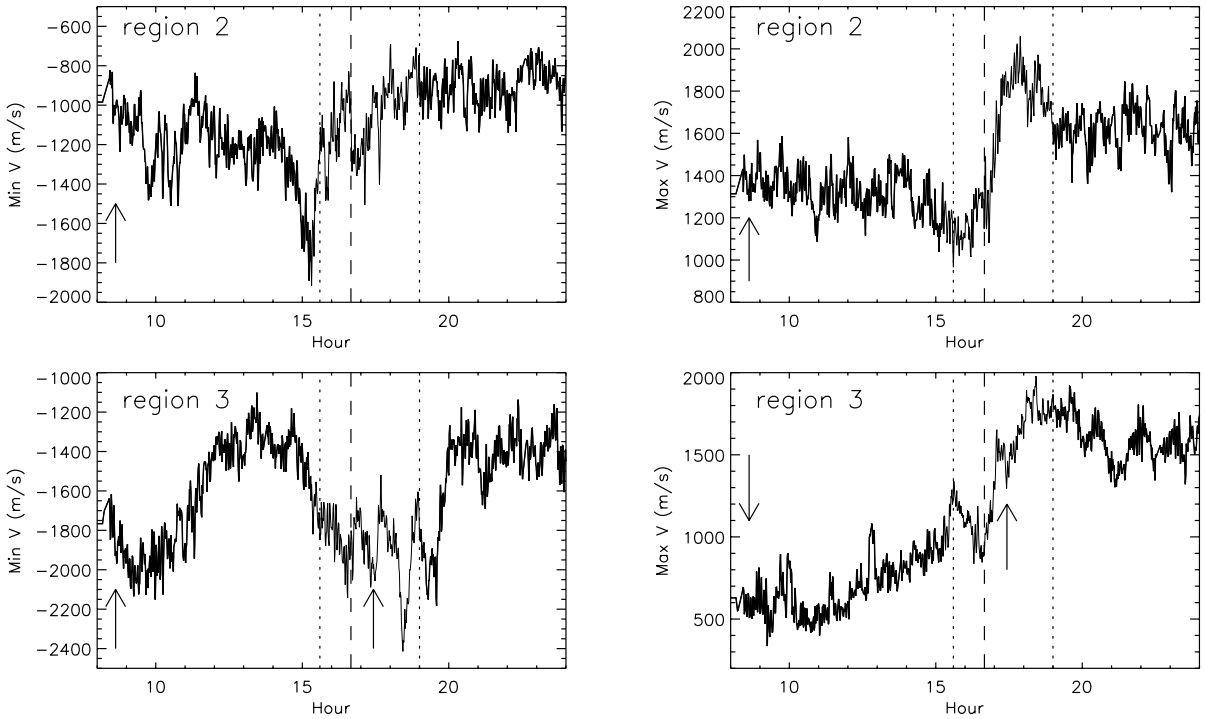

Fig. 7. Minimum (*left*) and maximum (*right*) velocity in regions 2 and 3 (numbers refers to regions defined in Fig. 4) from MDI data. The vertical dashed line marks the beginning of the Hα flare. The dotted line correspond to one hour before the beginning of the Hα flare and to 1.5 hour after its end. The arrows indicate that the region has been observed with THEMIS at that time. The projection effects are small.

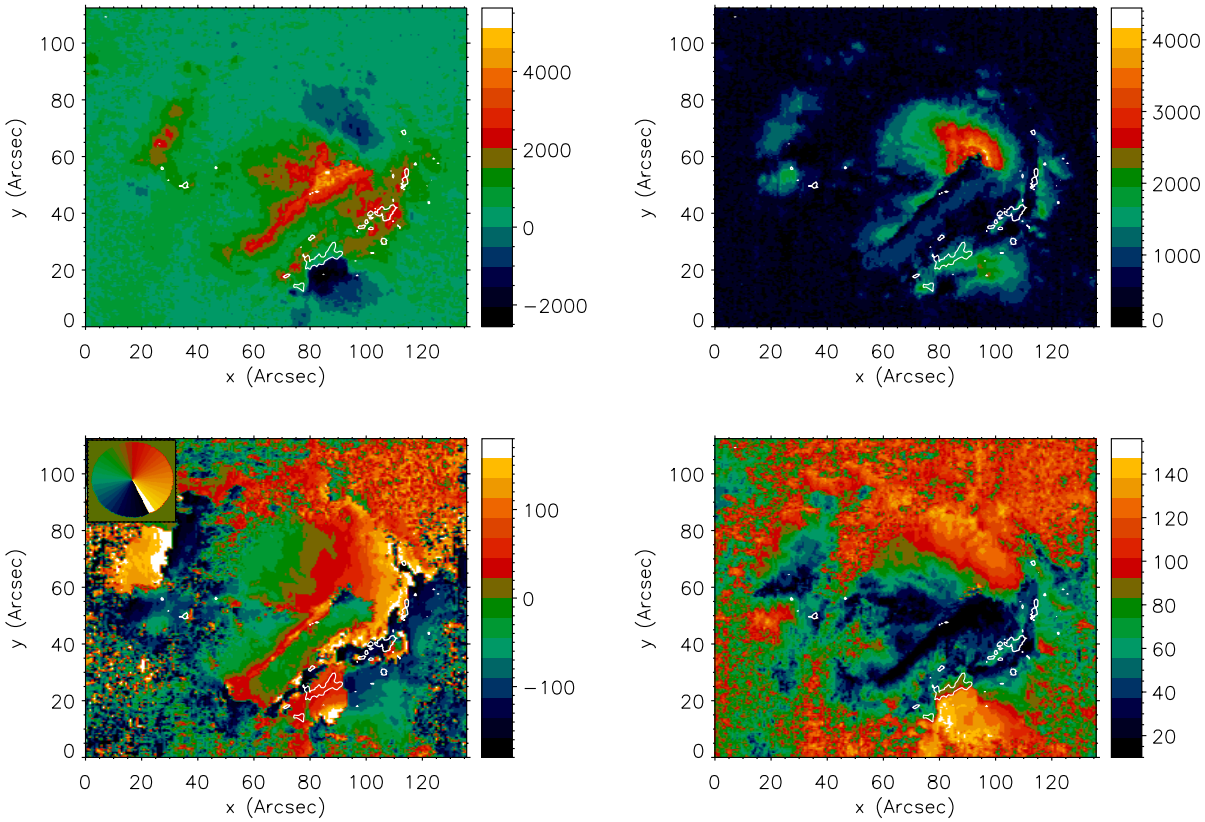

Fig. 8. Vertical magnetic field strength (*top left*, in G), horizontal magnetic field strength (*top right*, in G), azimuth (*bottom left*, in degrees), and inclination with respect to the vertical (*bottom right*, in degrees) for the Nov. 26 scan made at THEMIS (8:24), after correction of the 180° ambiguity (see text, Sect. 3.1) and projection effects, using the Mees Observatory code (see text). The reference for the azimuth is shown at the top of the plot. Thin white lines show the location of strong velocity flows (-2 km s^{-1}) corresponding to the blueshifted part of region 3. Thick white lines show the location of a strong Stokes V amplitude at ~300 mÅ from the line center (same as Fig. 6 top with umbra signal removed), corresponding to the strong flow in region 2.

have a similar behavior. These data are less noisy than the data obtained by scans, because we were able to average 125 spectra together. We observe a strong negative velocity of ∼3 km s^{-1} (blueshift, corresponding to upflow), which was already visible on the Nov. 26 scan (i.e. 9 hours before). This suggests that this is a long lived structure despite the occurrence of the flare in that region. However we also observe a strong positive velocity of ∼1.3 km s^{-1} which was not clearly visible on the morning scan. So, the region has significantly evolved over that time period, as can be seen in Fig. 3, which shows MDI maps at different times. These two velocity features are located North of the neutral line (next to the small spot of opposite polarity). The peaks of these two flows are separated by 11 arcsec and are quite stable during the 12 min of observations. The amplitudes of the peaks are also stable. However, some variations (1 km s^{-1} over 12 min) are seen in Fig. 9 at coordinates [40″, 47″] along the slit. Such variations could be related to the occurrence of the flare, and to changes observed in the MDI data after the flare on the scale of 1 hour in region 3.

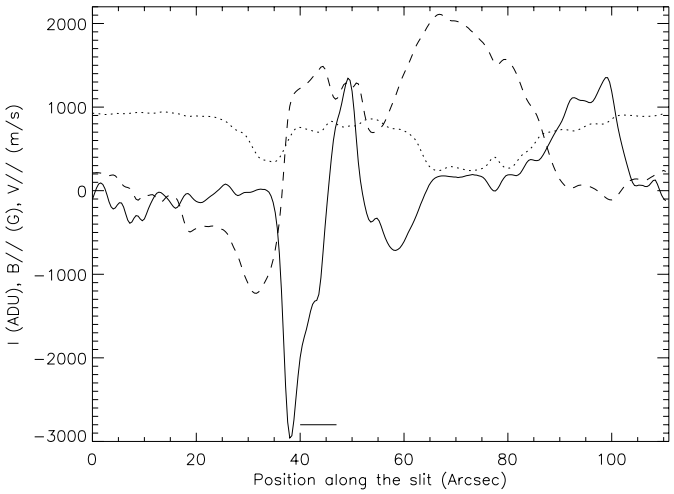

Fig. 9. LOS velocity field (solid line) from which the average has been subtracted, magnetic field (dashed line) and continuum intensity (dotted line) along the slit from THEMIS observation made at a fixed position on Nov. 26 (17:20 UT), using the Ni line. The small horizontal line correspond to the position where a variation over time is observed (see Sect. 4.3.1).

4.3.2. Fine structure of the flows

The line-of-sight magnetic and velocity fields shown in Fig. 9 are similar for all wavelengths of the data set. The 5635.8 and 5634.0 Å lines also show a double structure in the negative velocity flow region, which is clearly seen on several individual spectra. They are separated by a distance of 5 arcsec. There is probably a double structure in the positive velocity flow as well, visible on some individual spectra, with a separation of 1.5 to 3 arcsec. Given the relatively poor spatial resolution of these data, the difference in pointing due to the atmospheric refraction probably has a small effect. Therefore, it is likely that the more complex structure (with smaller features) is due to the low formation height of these lines.

The peak-to-peak amplitude of the velocity signal (which is independent of the chosen zero) varies with the wavelength: it is larger for the 5635.8 and 5634.0 Å lines (resp. 4.79 km s^{-1} and 4.58 km s^{-1}) and smaller for the other wavelengths (4.31 km s^{-1} for the Ni line and 4.00 km s^{-1} for the 6301.5 line). We exclude the 6302.5Å line from this comparison because the computation of the line-of-sight velocity is less reliable due to the presence of a telluric line across the shifted line. The maximum amplitude for the negative velocity field is also larger for the 5635.8 line (3.08 km s^{-1}), and smaller for the 6301.5 line. Again, this difference is probably due to the different height formation of these lines.

4.3.3. Stokes profile analysis and inversion results

The Stokes spectra for the Ni line in the region around the flare (after averaging over 125 frames, at 17:20) are shown in Fig. 10. Just above the LOS magnetic field reversal (position 8″), one can clearly see the strong negative velocity flows, previously seen in region 3. We also observe peculiar *Q* profiles, in particular for the Ni line, as shown in Fig. 10. A closer inspection of the *Q* profiles shows two components: one that would be blueshifted corresponding to LOS velocity of ∼5 km s^{-1}, and another to zero velocity. This feature is visible over several pixels along the slit and seems to form a coherent structure. These abnormal *Q* profiles were also observed in the morning scan 9 hours before, and, therefore, probably correspond to long-lived features. It is also very clearly visible in the 5634.0 and 5635.8 Å lines, which are formed deeper, but almost not visible in the 6301.5 line, and not visible at all in the 6302.5 line. The structure of the downflow region seems to be more simple, although the Stokes *U* profiles are quite complex.

From the computation of the vector magnetic field (using the first method with a single component only, see Sect. 4.2.2 and Fig. 8) for the morning scan, we find an average inclination of the negative velocity zone of about 84°, that is almost horizontal (90°). We also obtain a similar azimuth over the whole zone, in the range [60°, 70°]. If the flows are aligned with the magnetic field, this would correspond to a strong shear since the adjacent velocity components (of opposite sign) would be close to horizontal and in the same direction. The inclination with respect to the LOS is ∼58° in the region of large negative velocity flow, which gives amplitude of 9.4 km s^{-1} for a 5 km s^{-1} LOS component of flows. This is also supersonic. A MDI movie of the LOS magnetic field in the region does not show any motion of small magnetic features that would correspond to such an horizontal flow, but this could be due to the insufficient spatial resolution. The amplitude of this flow, integrated over the whole time period corresponds to a large distance, which may look surprising; if these observations correspond to downflows and upflows, for example, they would be more or less perpendicular to the magnetic field lines, which is also puzzling. However, the observations of such flows could mean that the magnetic field has unresolved filamentary structure allowing plasma to flow throw without disturbing the field lines.

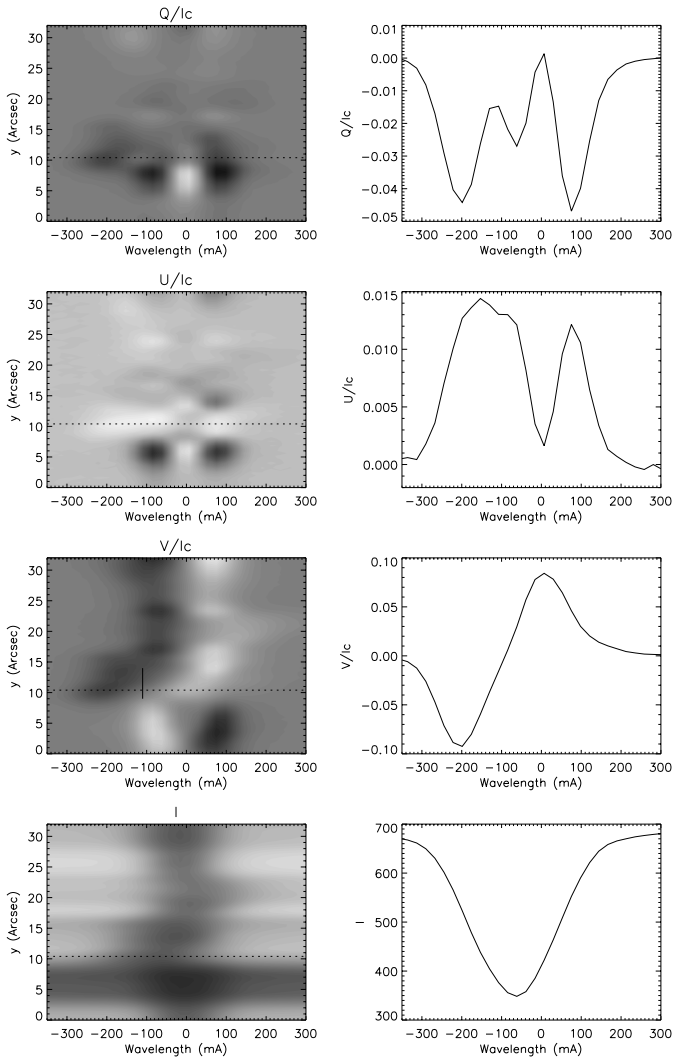

Fig. 10. *Left*: Stokes spectra for the Ni line in the flare region (the neutral line is at the bottom of that field-of-view) on Nov. 26 (17:20 UT). The y-axis is along the slit. I_c is the continuum intensity. The small vertical line on Stokes V indicates the position of the strong blueshifted flow. *Right*: Stokes spectra at the position indicated by the dotted line on the spectra on the left, where some unusual Q profiles are observed. The location of this cut is also shown in Fig. 2.

The full inversion using two magnetic components (in addition to the non-magnetic component) has been performed simultaneously for separate wavelengths, using the Ni line and the 6302.5/6301.5 Å lines and assuming that there is no depth dependence (except for the temperature). These lines give similar results. After correction for the projection effects (inclination) we find flows that are supersonic over the distance of 2–3 arcsec, the maximum flow being 7.7 km s^{-1}. The polarity of both magnetic components is the same than the main polarity. There is no difference in azimuth between the two magnetic components (although the azimuths differ from the previous computation by ∼30°). However the inclinations for the two magnetic components are quite different and differ by ∼36° from each other. The errorbars for the inclinations and azimuths are of the order of 1–2 degrees. They have similar filling factors (0.4) and similar magnetic fields. The microturbulence velocity seems to be larger for the blueshifted component, but this is more uncertain.

5. Summary and discussion

This paper presents new results from the first coordinated campaign between THEMIS (providing multiline spectropolarimetric data) and MDI (providing a high temporal cadence over a long period). We have observed two peculiar flows in AR 9236:

(i) *A supersonic downflow (10 km s^{-1}) mostly visible in Stokes V, inclined by 51° from the vertical*. The redshift is also visible in Stokes I, including the spectral line not sensitive to the magnetic field. The azimuth and inclination of this component differ from the non-shifted magnetic component and show a complex topology. This flow was observed only in the morning data of Nov. 26, 2000, in spectropolarimetric mode of THEMIS, and, unfortunately, no other THEMIS measurements are available. However, MDI observed this flow with reduced amplitude of 1.5–2 km s^{-1} (in region 2). Since this flow is visible in MDI data for at least 8 hours, we suggest that this flow is a long-lived downflow which is observed during its decaying phase. We do not have any explanation concerning the origin of this flow. It could originates in the previous Hα flare, which ended 5 hours before, or it could be related to the strong X-ray emission observed at that time (Fig. 1). Unfortunately we have not been able to establish with certainty that this strong X-ray flux is associated to this active region: H-α images from Learmonth Observatory do not show any enhancement at that time in this region nor in the other large active region present on the disk that day (AR 9240), while the radio flux from Nancay Observatory shows enhancements in both region. Therefore, the origin of this flow is still an open question. We note that the decreasing magnetic fluxes, both positive and negative, from 8:00 UT up to the beginning of the Hα flare are surprising because one would expect an increase in magnetic flux from a strong downflow (however, no converging pattern is visible either).

(ii) *A strong blueshifted flow adjacent to a strong redshifted flow, next to the neutral line.* For the same reasons than for the flow above, MDI data (region 3) suggest that this is a rather long-lived structures. Furthermore, THEMIS provided two observations of this flow, 9 hours apart, which also suggest that this was long-lived, although the global configuration of the LOS velocity field changed significantly over the day. If we make the assumption that these flows follow magnetic field lines, the magnetic topology of the region deduced from the inversion of the Stokes parameters observed with THEMIS suggests that these flows are close to horizontal and in the same direction, which can be interpreted as a horizontal shear, with one of the component (the blueshifted one) being supersonic over 2–3 arcsec. A shear of such amplitude has not been observed before in the photosphere. We cannot rule out a downflow (adjacent to an upflow) that would be almost horizontal instead of a shear, since the field lines are not strictly horizontal. The initial existence of this strong flow may be unrelated to the flare. However, the redshifted component increased by 800 m s^{-1} after the flare on the long time scale.

Therefore, this flow was influenced by the flare occurring in the region, and might play important role in the MHD process of restructuring of the magnetic configuration during the flare. The kinetic energy density of the flows was comparable with the magnetic energy density. Also, the changes of these quantities during the flare are also of the same order of magnitude. Preliminary Stokes profile inversions show that the supersonic component has an azimuth similar to the non-shifted component but a different LOS inclination, suggesting a complex topology as well. THEMIS observations also show that this flow presents some fine structures with scales in the range of 1–3 arcsec.

Supersonic flows in the photosphere have been observed by very few observers so far. Martinez Pillet et al. (1994) observed supersonic downflows in a δ-type spot at the location of polarity inversion, which they claim has nothing to do with a reconnection process because it is long-lived (more than 3 hours); the polarity of the shifted component is the same than the polarity of the non shifted component or opposite depending on the pixel. del Toro Iniesta et al. (2001) also observed a supersonic downflow in the penumbra of a simple sunspot using high resolution observations and a full inversion method, the downflow corresponding to a polarity opposite to that of the unshifted components. Our features are also different from mustaches which are very short-lived structures (5–10 min) as well as from Ellerman bombs (1–2 arcsec features). Our observations were made in different conditions and the features have different characteristics (very inclined flows one case, and different polarity properties). The supersonic flows are probably long-lived (8 hours at least), and the second one is modified at (or around) the time of the flare. Strong downflows and upflows have also been observed by Sigwarth (2001), with Stokes V profiles similar to ours with strongly shifted components (implying supersonic velocities) of either the same polarity or opposite polarities. His observations are associated with flux emergence and are interpreted as redshifted preshock and blueshifted postshock profiles.

It could seem surprising that flows of such amplitude have been rarely observed before at the photospheric level, but spectropolarimetric observations of solar flares using spectral lines formed in the photosphere are not very common, which make these new results very important. The origin of these strong flows is not clear at this stage, and would request more observations in similar conditions with a better coordination with chromospheric observations to see if they are affected by the flare or if they are related to the triggering of the flare.

For another improvement to this analysis, it is the necessity to make robust inversions of Stokes profiles. This is critical for the interpretation. The results presented in this paper confirm the existence of a 10 $\mathrm{km\,s^{-1}}$ LOS flow for example, and show that the strong downflow probably exhibits a complex fine structure over the field of 2×5 arcsec^2. However more work needs to be done on these data to compare the Stokes parameters at all wavelengths to be able to derive the variation of these strong flows with height in the photosphere: this is a work in progress. Note that the line profile inversions with a depth dependence did not improve the fit; therefore, it is difficult at this point to conclude if the differences for the different wavelengths are due to strong vertical or horizontal gradients. We would also like to point out that we observed very interesting features in Stokes spectra provided by the Ni line as well as with lines with a small Lande factor, and that the inversion using the Fe lines and the Ni line gave similar results.

Acknowledgements. We thank F. Paletou, our resident astronomer during the THEMIS observations, J. Arnaud for his help with the data processing and fruitful discussions, T. Metcalf for providing some codes to compute the vector magnetic fields. We also thank S. Solanki and A. Lagg for providing their inversion code and for taking some time to explain to us how to use it. We thank K. Puschmann who kindly provided the line formation depths of Table 2. The THEMIS telescope is operated on the Tenerife island by CNRS-CNR in the Spanish Observatorio del teide of the Instituto de Astrofísica de Canarias. SOHO is a mission of international cooperation between the European Space Agency (ESA) and NASA. This study is also based on Hα data obtained at OAFA (El Leoncito, San Juan, Argentina) in the framework of the German-Argentinean HASTA/MICA Project, a collaboration of MPE, IAFE, OAFA and MPAe. GOES data have been provided by the Space Environment Center (National Oceanic and Atmospheric Administration). Trips to Stanford were financed by the PNST (Programme National Soleil-Terre).

References

Canfield, C., de La Beaujardière, J.-F., Fan, Y., et al. 1993, ApJ, 411, 363
del Toro Iniesta, J. C., Bellot Rubio, L. R., & Collados, M. 2001, ApJ, 549, L139
Fruttiger, C. 2000, Inversion of Zeeman Split Stokes Profiles, Ph.D. Thesis
Harvey, K. L., & Harvey, J. W. 1976, Sol. Phys., 47, 233
Jefferies, J., Lites, B. W., & Skumanich, A. 1989, ApJ, 343, 920
Jones, H. 1989, Sol. Phys., 120, 211
Keil, S. L., Balasubramaniam, K. S., Bernasconi, P., Smaldone, L. A., & Cauzzi, G. 1994, 14th NSO/Sacramento Peak Summer Workshop, ASP Conf. Ser., 68, 265
Kentischer, T. J., & Mattig, W. 1995, A&A, 300, 539
Kosovichev, A. G., & Zharkova, V. V. 2001, ApJ, 550, L105
López Ariste, A., Rayrole, J., & Semel, M. 2000, A&AS, 142, 137
Martinez Pillet, V., Lites, B. W., Skumanich, A., & Degenhardt, D. 1994, ApJ, 425, L113
Martres, M. J., & Soru-Escaut, I. 1977, Sol. Phys., 53, 225
Meunier, N., Arnaud, J., & Vigneau, J. 2002, Il Nuevo Cimento C, 25C(5-6), 659
Paletou, F., & Molodij, G. 2000, 20th NSO/Sacramento Peak Summer Workshop, ASP Conf. Ser., 236, 9
Rees, D., & Rayrole, J. 1979, A&A, 74, 1
Severny, A. B. 1958, Izv. Krym. Astr. Obs., 20, 22
Scherrer, P. H., Bogart, R. S., Bush, R. I., et al. 1995, Sol. Phys., 162, 129
Sigwarth, M. 2001, ApJ, 563, 1031
Yoshimura, H., Tanaka, K., Skimizu, M., & Hiei, E. 1971, Publ. Astr. Soc. Japan, 23, 443